Hole-Conductor-Free Mesoscopic TiO2/CH3NH3PbI3 Heterojunction Solar Cells Based on Anatase Nanosheets and Carbon Counter Electrodes

ARTICLE *in* JOURNAL OF PHYSICAL CHEMISTRY LETTERS · JUNE 2014

Impact Factor: 7.46 · DOI: 10.1021/jz500833z

8 AUTHORS, INCLUDING:

Yaoguang Rong
Huazhong University of Science and Technology
34 PUBLICATIONS **753** CITATIONS
SEE PROFILE

Tongfa Liu
Huazhong University of Science and Technology
18 PUBLICATIONS **496** CITATIONS
SEE PROFILE

Xiong Li
École Polytechnique Fédérale de Lausanne
43 PUBLICATIONS **625** CITATIONS
SEE PROFILE

Hongwei Han
Huazhong University of Science and Technology
78 PUBLICATIONS **1,678** CITATIONS
SEE PROFILE

THE JOURNAL OF PHYSICAL CHEMISTRY Letters

Letter

pubs.acs.org/JPCL

Hole-Conductor-Free Mesoscopic $TiO_2/CH_3NH_3PbI_3$ Heterojunction Solar Cells Based on Anatase Nanosheets and Carbon Counter Electrodes

Yaoguang Rong,† Zhiliang Ku,† Anyi Mei, Tongfa Liu, Mi Xu, Songguk Ko, Xiong Li, and Hongwei Han*

Michael Grätzel Center for Mesoscopic Solar Cells, Wuhan National Laboratory for Optoelectronics, School of Optical and Electronic Information, Huazhong University of Science and Technology, Wuhan, Hubei 430074, People's Republic of China

Supporting Information

ABSTRACT: A hole-conductor-free fully printable mesoscopic $TiO_2/CH_3NH_3PbI_3$ heterojunction solar cell was developed with TiO_2 nanosheets containing high levels of exposed (001) facets. The solar cell embodiment employed a double layer of mesoporous TiO_2 and ZrO_2 as a scaffold infiltrated by perovskite as a light harvester. No hole conductor or Au reflector was employed. Instead, the back contact was simply a printable carbon layer. The perovskite was infiltrated from solution through the porous carbon layer. The high reactivity of (001) facets in TiO_2 nanosheets improved the interfacial properties between the perovskite and the electron collector. As a result, photoelectric conversion efficiency of up to 10.64% was obtained with the hole-conductor-free fully printable mesoscopic $TiO_2/CH_3NH_3PbI_3$ heterojunction solar cell. The advantages of fully printable technology and the use of low-cost carbon-materials-based counter electrode and hole-conductor-free structure provide this design a promising prospect to approach low-cost photovoltaic devices.

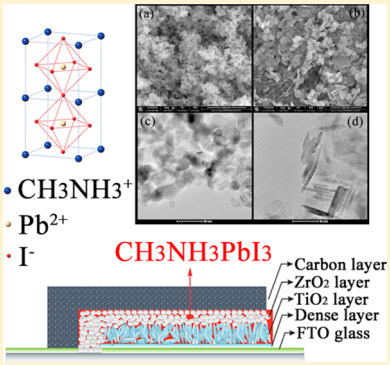

SECTION: Energy Conversion and Storage; Energy and Charge Transport

In the past decade, extensive research has been concentrated on the development of renewable energy. Among them, photovoltaics have been considered as the most promising technology due to their availability, sustainability, and reliability. However, the conventional solar cells, such as those dominant currently in photovoltaic industry silica solar cells, seem to be difficult to meet the market demand for low-cost devices on account of high raw material cost and complex manufacturing processes.[1,2] To reduce the cost of photovoltaic devices, an efficient strategy is to relax the quality requirements of raw materials and simplify the fabrication procedures. Due to meeting these demands, dye-sensitized solar cells (DSSCs) have attracted much attention since reported by the M. Grätzel group in 1991.[3] Usually, DSSCs contain a mesoscopic working electrode (such as TiO_2) sensitized with a dye, a liquid-state electrolyte containing a redox couple, and a platinized counter electrode (CE).[4,5] Indeed, the problems associated with electrolyte leakage, dye desorption, and electrode corrosion have limited its applications. Replacing the liquid-state electrolytes with solid-state intermedium such as hole-transporting materials (HTMs) to fabricate all-solid-state DSSCs seems to be a solution to these problems.[6−8] Unfortunately, these devices still could not obtain competitive photovoltaic performance compared with the conventional photovoltaics.[9]

Mesoscopic perovskite solar cells, evolved from DSSCs, are an exciting class of photovoltaics that could fulfill these requirements mentioned above.[10−14] They employ organometal trihalide perovskite absorbers such as $CH_3NH_3PbX_3$ (X = Cl, Br, I) instead of the dyes in DSSCs to deliver all-solid-state photovoltaic devices with a power conversion efficiency (PCE) beyond 15%.[12,13] However, it should be noted that all of these devices used gold or silver as the back contact in conjunction with HTMs acting as electron blocking layers. HTMs such as 2,2′,7,7′-tetrakis(*N*,*N*-di-*p*-methoxyphenylamine)-9,9′-spirobifluorene (spiro-OMeTAD) are quite expensive at present and would limit its use in wide application. Besides, the vacuum deposition process for the noble-metal-based CEs is also highly energy consuming. Obviously, it is worth developing HTM-free mesoscopic perovskite solar cells and replacing the noble-metal-based CEs with inexpensive and abundantly available materials.

Previously, we have reported full printable processed mesoscopic $CH_3NH_3PbI_3/TiO_2$ heterojunction solar cells with carbon CEs.[15] Employing a common drop-coating method to infiltrate the perovskite $CH_3NH_3PbI_3$ into the three porous layers, the device without a HTM layer showed a PCE of 6.64%. Though the efficiency was not as high as that obtained by devices fabricated with HTM and Au CEs, this design still shows the prospect for ultimate low-cost photovoltaic devices with inexpensive CEs and a printable fabrication process.

As nanostructured solar cells, the potential for future increases in efficiency of mesoscopic perovskite solar cells may largely rely on the development of material nanoachitectures. With this as motivation, various wide-band-gap

Received: April 29, 2014
Accepted: June 6, 2014
Published: June 6, 2014

   dx.doi.org/10.1021/jz500833z | *J. Phys. Chem. Lett.* 2014, 5, 2160−2164

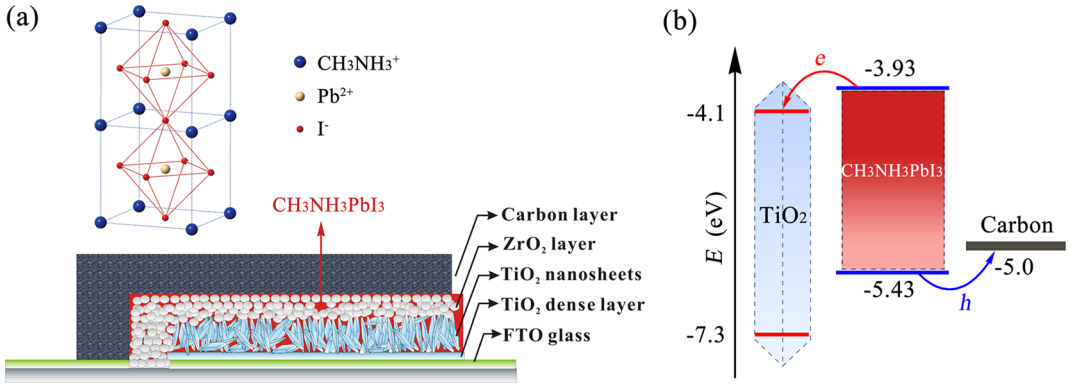

Figure 1. (a) Schematic of a hole-conductor-free mesoscopic $TiO_2/CH_3NH_3PbI_3$ heterojunction solar cell based on anatase NSs and carbon CEs. (b) Energy level diagram of a $TiO_2/CH_3NH_3PbI_3$ heterojunction solar cell based on a carbon CE.

oxide semiconductors with different architectures such as nanowires, nanosheets (NSs), and nanorods have been applied in DSSCs.[16−20] Studies have shown that the (001) facets of anatase TiO_2 are more reactive than the (101) facets,[21] and it was proposed that the higher ionic charge of the exposed (001) would strengthen the attachment of the light absorbers to the TiO_2 surface, thereby facilitating the electrons injected in the conduction band of the oxide.[17,18]

Herein, we report TiO_2 NSs with high levels of exposed (001) facets employed as the electron collector in hole-conductor-free mesoscopic heterojunction solar cells based on carbon CEs. With a two-step sequential method to infiltrate the perovskite $CH_3NH_3PbI_3$, the mesoscopic solar cells using TiO_2 NSs as the electron collectors achieved a remarkable PCE of up to 10.64% under simulated AM1.5 one sun illumination, which was 45% higher than that of devices based on Degussa P25 TiO_2 nanoparticles (NPs).

The schematic of a typical hole-conductor-free mesoscopic $TiO_2/CH_3NH_3PbI_3$ heterojunction solar cell based on a carbon CE is shown in Figure 1a. Indeed, all of the films in the mesoscopic solar cell could be fabricated by screen-printing technology including the mesoscopic carbon CE. We fabricated 4 × 5 devices on a single fluorine-doped tin oxide (FTO) glass substrate to ensure the thicknesses of each layer in the devices were controllable.[22] FTO glass plates with high transparency in the visible range were purchased from CSG Holding Co. Ltd. It is worth mentioning that the TiO_2 film and the mesoscopic carbon CE were separated by the porous ZrO_2 layer, ensuring that there was no risk of direct contact between the photoanode and CE.[23,24] Moreover, the distance of the spacer layer, which affects the series resistance of the device, would be controlled precisely by the thickness of the porous ZrO_2 layer with the technology of screen-printing.

Figure 1b shows the energy level diagram of this hole-conductor-free mesoscopic $TiO_2/CH_3NH_3PbI_3$ heterojunction solar cell. Once the perovskite $CH_3NH_3PbI_3$ in the porous layers absorbs light, electron−hole pairs are generated with the electron on the conduction band (−3.93 eV) and the hole on the valence band (−5.43 eV) of the perovskite. Immediately, the electron−hole pairs separate by injecting an electron into TiO_2 (−4.0 eV) and transporting the hole to the carbon CE (−5.0 eV) and then forming photocurrent in the device.

TiO_2 NSs were synthesized via a simple hydrothermal rout using tetrabutyl titanate as the precursor and HF solution as the solvent. With the treatment of HF solution, the TiO_2 crystals may have larger size along the *a* axis and expose more (001) facets, resulting in a shape transformation from an octahedral bipyramid to truncated octahedral bipyramid and finally to a NS,[25,26] as shown in Figure S1 (Supporting Information). X-ray diffraction (XRD) patterns of the NSs and Degussa P25 TiO_2 NPs are shown in Figure 2. All of the diffraction peaks are

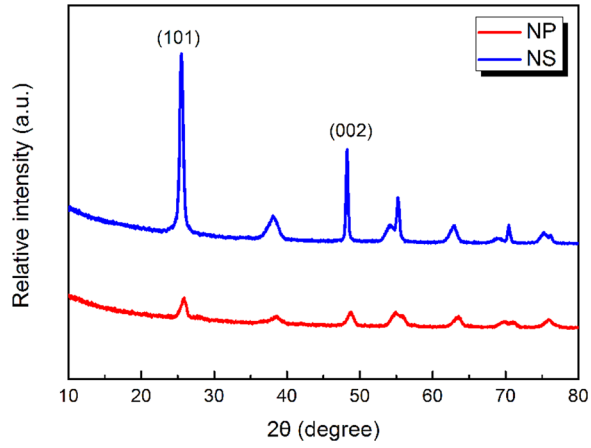

Figure 2. XRD patterns of Degussa P25 TiO_2 NPs and synthesized TiO_2 NSs.

indexed to the anatase phase of TiO_2 (JCPDS No. 21-1272), indicating that the obtained products are pure anatase TiO_2 crystals. Compared with the NP, the NS possesses stronger and sharper (101) and (002) diffraction peaks. This indicates a preferential growth along the [100] direction with the treatment of HF solution.

Figure 3 shows the scanning electron microscopy (SEM) and transmission electron microscope (TEM) images of TiO_2 NPs and NSs. For the SEM images, being different from the spherical or rod-shaped particles of the Degussa P25 TiO_2 version, the synthesized TiO_2 NS distributes uniformly in a sheet-like morphology with a ∼80 nm side length. These results are quite in accordance with the XRD patterns. The detailed morphology of the synthesized TiO_2 NS could be observed in TEM images. Compared with the P25 TiO_2 NP, theTiO_2 NS shows a rectangular outline in the section direction with a thickness of ∼8 and an 80 nm side length, which is well in agreement with SEM results. As reported,[25] the percentage of (001) can be calculated by the following equation

$$\eta = \frac{2 \times A^2}{2 \times A^2 + 4 \times A \times H} \quad (1)$$

dx.doi.org/10.1021/jz500833z | J. Phys. Chem. Lett. 2014, 5, 2160−2164

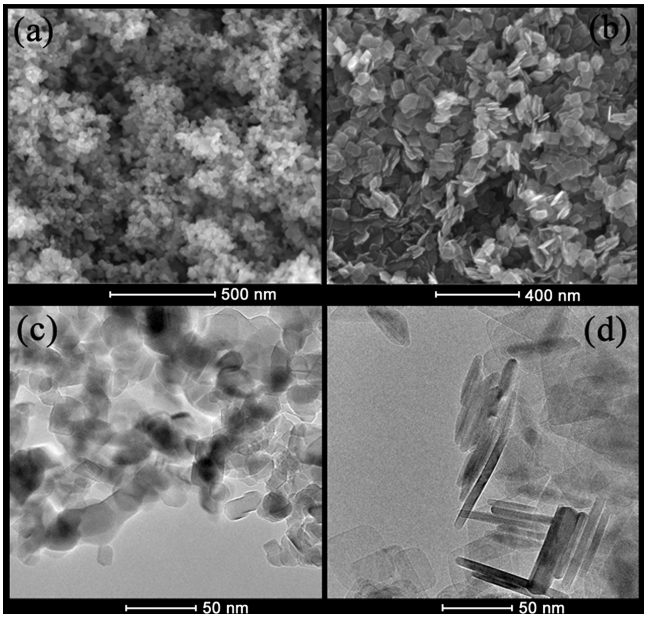

Figure 3. SEM images of (a) P25 TiO_2 NPs and (b) synthesized TiO_2 NSs; TEM images of (c) NPs and (d) NSs.

where η is the percentage of (001), A is the side length, and H is the thickness of the NS. It was found that the percentage of (001) facets, estimated by eq 1, of the synthesized TiO_2 NS was as high as 83.3%, while the percentage of (001) facets in the TiO_2 NP is commonly less than 10%.[27]

The synthesized TiO_2 NS was employed as the host of perovskite $CH_3NH_3PbI_3$ to fabricate mesoscopic heterojunction solar cells. First, we have compared the drop-coating method and two-step sequential method for depositing $CH_3NH_3PbI_3$. The absorption spectra of TiO_2 NS and NP films coated with perovskite were presented in Figure S2 (Supporting Information), in which the absorbance of sample using the sequential method is much higher than that of the sample using the drop-coating method in the range of from 500 to 800 nm. This result indicated that the sequential method could obtain more $CH_3NH_3PbI_3$ loading amount in the porous TiO_2 films and then a stronger light harvesting ability compared with the drop-coating method.[28] Indeed, compared with the device fabricated using the drop-coating method, the darker uniform color could be found in the digital image of the device fabricated using the two-step sequential method, as presented in the inset image of Figure S2 (Supporting Information). The enhancement of the light-harvesting efficiency obtained with the sequential method would result in a larger short-circuit current density (J_{sc}) for the device. Therefore, in the following work, we fabricated the mesoscopic heterojunction solar cells with the perovskite deposited by the two-step sequential method.

The representative $J-V$ curves of the mesoscopic TiO_2/$CH_3NH_3PbI_3$ heterojunction solar cells based on P25 TiO_2 NPs and TiO_2 NSs are presented in Figure 4a. Clearly, under AM1.5 simulated sunlight of 100 mW cm^{-2}, the device based on the P25 TiO_2 NP exhibited an open-circuit voltage (V_{oc}) of 0.839 V, a J_{sc} of 13.7 mA cm^{-2}, and a fill factor (FF) of 0.64, yielding a PCE of 7.36%. Interestingly, the mesoscopic heterojunction solar cell based on the synthesized TiO_2 NS exhibited a much higher J_{sc} of 20.1 mA cm^{-2}, which was almost 47% higher than that of the NP-based device, leading to a PCE of up to 10.64%. To check the reproducibility of device performance, histograms for photovoltaic parameters of devices based on NPs and NSs are presented in Figure S3 (Supporting Information).

The incident photon-to-current conversion efficiency (IPCE) specifies the ratio of extracted electrons to incident photons at a given wavelength, which reflects the light response of the devices and is directly related to the J_{sc}. The IPCE spectra of the mesoscopic heterojunction solar cells based on TiO_2 NPs and NSs are presented in Figure 4b. Normally, the mesoscopic TiO_2/$CH_3NH_3PbI_3$ heterojunction solar cells show excellent photocurrent response from 400 to 800 nm, with IPCE reaching a maximum at the wavelengths between 450 and 500 nm and then decreasing at longer wavelengths until 800 nm. Compared with the mesoscopic heterojunction solar cell with P25 TiO_2 NP films, device using synthesized TiO_2 NS films exhibit much higher IPCE, which reached over 85% at the wavelength range of 450−500 nm and over 60% at almost the entire wavelength range of 400−750 nm, which were in reasonable agreement with the measured values of J_{sc}. Notice, J_{sc} is proportional to IPCE, where IPCE is the product of the light-harvesting efficiency (η_{lh}), electron injection efficiency (η_{inj}), and charge collection efficiency (η_{cc}). η_{lh} is determined by the absorption of the sensitizer, where perovskite $CH_3NH_3PbI_3$

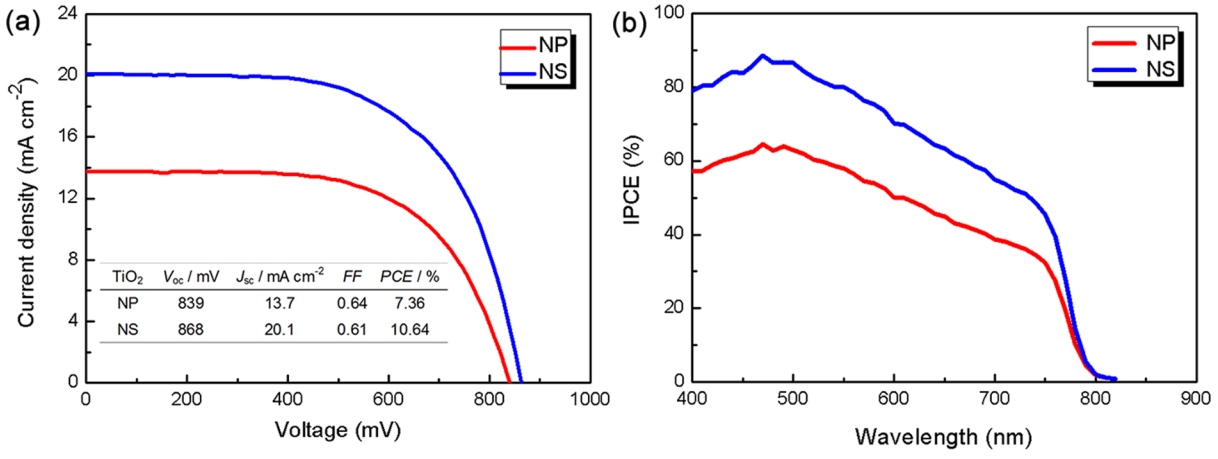

Figure 4. (a) $J-V$ curves under AM1.5 simulated sunlight of 100 mW cm^{-2} and (b) IPCE spectra of the mesoscopic TiO_2/$CH_3NH_3PbI_3$ heterojunction solar cells based on P25 TiO_2 NPs and TiO_2 NSs.

dx.doi.org/10.1021/jz500833z | J. Phys. Chem. Lett. 2014, 5, 2160−2164

presents a molar extinction coefficient of about 1.5×10^5 M^{-1} cm^{-1} at 550 nm, which is 2−3 times higher than those of organic dyes such as D149 with 6.9×10^4 M^{-1} cm^{-1} at 526 nm and Y123 with 5.3×10^4 M^{-1} cm^{-1} at 532 nm. Because the TiO_2 films were deposited with identical thicknesses and presented similar microstructures, η_{lh} would be similar, which has been confirmed by absorption spectra of TiO_2 films coated with perovskite, as shown in Figure S2 (Supporting Information), and is irrelevant to the change in J_{sc}. Indeed, η_{inj} is directly affected by the interfacial properties between the perovskite and the TiO_2 electron collectors. It is proposed that the higher concentration of ionic charge of the exposed (001) facets in synthesized TiO_2 NSs, compared with TiO_2 NPs, would strengthen the attachment of the perovskite onto the TiO_2 surface and screen the electrons injected in the conduction band of the oxide, thus leading to a higher η_{inj} and then enhanced J_{sc} of the devices.[17,18]

To further investigate the charge transport process in the devices, impedance spectroscopy (IS) measurements were carried out with a potentiostat. It has been reported that in the IS spectra of typical lead iodide perovskite solar cells with a structure of TiO_2/perovskite/HTM/CE, there are mainly three RC elements representing the charge transfer resistance and recombination at TiO_2/perovskite, TiO_2/HTM, and HTM/CE interfaces.[29−32] In our case, because $CH_3NH_3PbI_3$ acted as a light absorber and at the same time as a hole conductor, we should only be concerned with the RC elements at TiO_2/perovskite and perovskite/CE interfaces. In the IS measurements, when we decreased the forward bias, the first semicircle at the high-frequency region remained almost unchanged, while the second semicircle at the low-frequency region increased in diameter significantly, as shown in Figure S4 (Supporting Information). Thus, it could be concluded that the first semicircle represented the impedance at the perovskite/CE interface, and the second semicircle represented the impedance at the TiO_2/perovskite interface.

Figure 5 shows the Nyquist plots obtained with devices using the P25 TiO_2 NP and synthesized TiO_2 NS as the electron collectors, and the equivalent circuit is presented in the inset. With a forward bias of 0.6 V, two well-defined semicircles could be observed in the range of 1 MHz to 100 mHz. Generally, the device using the TiO_2 NS possessed a smaller semicircle in the high-frequency region and a larger semicircle in the low-frequency region, indicating smaller charge transfer resistance at the perovskite/CE interface and larger recombination resistance at the TiO_2/perovskite interface. This result is consistent, on one hand, with the shape of the $J-V$ curves and, on the other, with the differences of V_{oc} observed in Figure 4a. It was proposed that the high percentage of exposed (001) facets in the synthesized TiO_2 NS would strengthen the attachment of the perovskite to the TiO_2 surface and thus improve the photogenerated current of the device. Meanwhile, it seemed that the use of the TiO_2 NS would not cause an increase of recombination between the electron collector and light absorber. It was supposed that the increased ionic charge of the (001) facets served to screen electrons in the TiO_2, leading to decreased recombination.[17,18] Therefore, the employment of TiO_2 NSs in such hole-conductor-free mesoscopic TiO_2/$CH_3NH_3PbI_3$ heterojunction solar cells led to enhancements in both J_{sc} and V_{oc}, yielding a PCE of up to 10.64%.

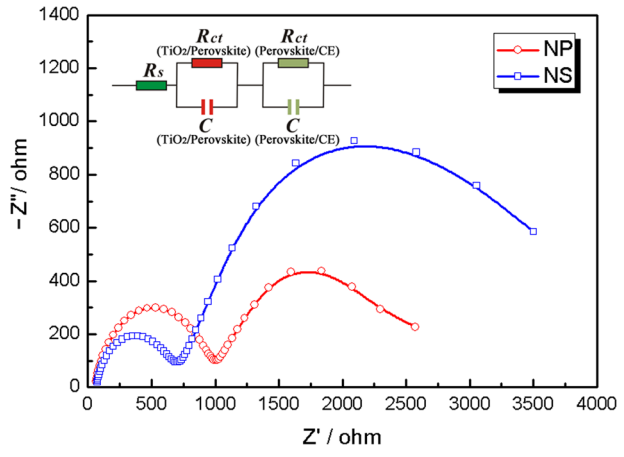

Figure 5. Nyquist plots of devices using P25 TiO_2NPs and synthesized TiO_2 NSs as the electron collectors and the equivalent circuit employed to fit the spectra. The IS measurements were carried out in the dark with a bias of 0.6 V.

In conclusion, TiO_2 NSs with a high percentage of exposed (001) facets were synthesized and employed as the electron collector in the hole-conductor-free mesoscopic TiO_2/$CH_3NH_3PbI_3$ heterojunction solar cells based on carbon CEs. The results indicate that the high reactivity of (001) facets in TiO_2 NSs improves the interfacial properties between the perovskite and the electron collector. As a result, an impressive PCE value exceeding 10.64% has been obtained by TiO_2 NSs/$CH_3NH_3PbI_3$ heterojunction solar cells with a two-step sequential method. Higher efficiency could be expected with the hole-conductor-free mesoscopic heterojunction solar cells through further optimizing the TiO_2 NSs containing high levels of exposed (001) facets. Meanwhile, the advantages of using low-cost carbon-materials-based CEs and a hole-conductor-free structure provide this design a promising prospect to approach low-cost photovoltaic devices.

■ ASSOCIATED CONTENT

Supporting Information

Synthesis of TiO_2 nanosheets, device fabrication and measurements, comparison of the drop-coating method and two-step sequential deposition method, and impedance spectroscopy measurements. This material is available free of charge via the Internet at http://pubs.acs.org.

■ AUTHOR INFORMATION

Corresponding Author

*E-mail: hongwei.han@mail.hust.edu.cn.

Author Contributions

†Y.R. and Z.K. contributed equally in this work.

Notes

The authors declare no competing financial interest.

■ ACKNOWLEDGMENTS

The authors acknowledge the financial support from the Ministry of Science and Technology of China (863, No. SS2013AA50303), the National Natural Science Foundation of China (Grant No. 61106056), the Science and Technology Department of Hubei Province (No. 2013BAA090), and the Fundamental Research Funds for the Central Universities (HUSTNY022). We also thank the Analytical and Testing Center of Huazhong University of Science and Technology (HUST) for X-ray diffraction (XRD) testing and the Center for Nanoscale Characterization & Devices (CNCD), WNLO of

HUST for field emission scanning electron microscopy (FE-SEM) and transmission electron microscopy (TEM).

REFERENCES

(1) Grätzel, M.; Janssen, R. A. J.; Mitzi, D. B.; Sargent, E. H. Materials Interface Engineering for Solution-Processed Photovoltaics. *Nature* **2012**, *448*, 304−312.

(2) Hardin, B. E.; Snaith, H. J.; McGehee, M. D. The Renaissance of Dye-Sensitized Solar Cells. *Nat. Photonics* **2012**, *6*, 162−169.

(3) O'Regan, B.; Grätzel, M. A Low-Cost, High-Efficiency Solar Cell Based on Dye-Sensitized Colloidal TiO_2 Films. *Nature* **1991**, *353*, 737−740.

(4) Hagfeldt, A.; Boschloo, G.; Sun, L.; Kloo, L.; Pettersson, H. Dye-Sensitized Solar Cells. *Chem. Rev.* **2010**, *110*, 6595−6663.

(5) Ito, S.; Murakami, T. N.; Comte, P.; Liska, P.; Grätzel, C.; Nazeeruddin, M. K.; Grätzel, M. Fabrication of Thin Film Dye Sensitized Solar Cells with Solar to Electric Power Conversion Efficiency over 10%. *Thin Solid Films* **2008**, *516*, 4613−4619.

(6) Bach, U.; Lupo, D.; Comte, P.; Moser, J. E.; Weissörtel, F.; Salbeck, J.; Spreitzer, H.; Grätzel, M. Solid-State Dye-Sensitized Mesoporous TiO_2 Solar Cells with High Photon-to-Electron Conversion Efficiencies. *Nature* **1998**, *395*, 583−585.

(7) Ding, I.-K.; Zhu, J.; Cai, W.; Moon, S.-J.; Cai, N.; Wang, P.; Zakeeruddin, S. M.; Grätzel, M.; Brongersma, M. L.; Cui, Y.; McGehee, M. D. Plasmonic Dye-Sensitized Solar Cells. *Adv. Energy Mater.* **2011**, *1*, 52−57.

(8) Rong, Y.; Li, X.; Ku, Z.; Liu, G.; Wang, H.; Xu, M.; Liu, L.; Hu, M.; Xiang, P.; Zhou, Z.; et al. Monolithic All-Solid-State Dye-Sensitized Solar Module Based on Mesoscopic Carbon Counter Electrodes. *Sol. Energy Mater. Sol. Cells* **2012**, *105*, 148−152.

(9) Green, M. A.; Emery, K.; Hishikawa, Y.; Warta, W.; Dunlop, E. D. Solar Cell Efficiency Tables (Version 43). *Prog. Photovolt: Res. Appl.* **2014**, *22*, 1−9.

(10) Kim, H.-S.; Lee, C.-R.; Im, J.-H.; Lee, K.-B.; Moehl, T.; Marchioro, A.; Moon, S.-J.; Humphry-Baker, R.; Yum, J.-H.; Moser, J. E.; et al. Lead Iodide Perovskite Sensitized All-Solid-State Submicron Thin Film Mesoscopic Solar Cell with Efficiency Exceeding 9%. *Sci. Rep.* **2012**, *2*, 591.

(11) Lee, M. M.; Teuscher, J.; Miyasaka, T.; Murakami, T. N.; Snaith, H. J. Efficient Hybrid Solar Cells Based on Meso-Superstructured Organometal Halide Perovskites. *Science* **2013**, *338*, 643−647.

(12) Burschka, J.; Pellet, N.; Moon, S.-J.; Humphry-Baker, R.; Gao, P.; Nazeeruddin, M. K.; Grätzel, M. Sequential Deposition as a Route to High-Performance Perovskite-Sensitized Solar Cells. *Nature* **2013**, *499*, 316−319.

(13) Liu, M.; Johnston, M. B.; Snaith, H. J. Efficient Planar Heterojunction Perovskite Solar Cells by Vapour Deposition. *Nature* **2013**, *501*, 395−398.

(14) Ball, J. M.; Lee, M. M.; Hey, A.; Snaith, H. J. Low-Temperature Processed Meso-Superstructured to Thin-Film Perovskite Solar Cells. *Energy Environ. Sci.* **2013**, *6*, 1739−1743.

(15) Ku, Z.; Rong, Y.; Xu, M.; Liu, T.; Han, H. Full Printable Processed Mesoscopic $CH_3NH_3PbI_3/TiO_2$ Heterojunction Solar Cells with Carbon Counter Electrode. *Sci. Rep.* **2013**, *3*, 3132.

(16) Law, M.; Greene, L. E.; Johnson, J. C.; Saykally, R.; Yang, P. Nanowire Dye-Sensitized Solar Cells. *Nat. Mater.* **2005**, *4*, 455−459.

(17) Etgar, L.; Zhang, W.; Gabriel, S.; Hickey, S. G.; Nazeeruddin, M. K.; Eychmüller, A.; Liu, B.; Grätzel, M. High Efficiency Quantum Dot Heterojunction Solar Cell Using Anatase (001) TiO_2 Nanosheets. *Adv. Mater.* **2012**, *24*, 2202−2206.

(18) Etgar, L.; Gao, P.; Xue, Z.; Peng, Q.; Chandiran, A. K.; Liu, B.; Nazeeruddin, M. K.; Grätzel, M. Mesoscopic $CH_3NH_3PbI_3/TiO_2$ Heterojunction Solar Cells. *J. Am. Chem. Soc.* **2012**, *134*, 17396−17399.

(19) Kim, H.-S.; Lee, J.-W.; Yantara, N.; Boix, P. P.; Kulkarni, S. A.; Mhaisalkar, S.; Grätzel, M.; Park, N.-G. High Efficiency Solid-State Sensitized Solar Cell-Based on Submicrometer Rutile TiO_2 Nanorod and $CH_3NH_3PbI_3$ Perovskite Sensitizer. *Nano Lett.* **2013**, *13*, 2412−2417.

(20) Varghese, O. K.; Paulose, M.; Grimes, C. A. Long Vertically Aligned Titania Nanotubes on Transparent Conducting Oxide for Highly Efficient Solar Cells. *Nat. Nanotechnol.* **2009**, *4*, 592−597.

(21) Kavan, L.; Grätzel, M.; Gilbert, S. E.; Klemenz, C.; Scheel, H. J. Electrochemical and Photoelectrochemical Investigation of Single-Crystal Anatase. *J. Am. Chem. Soc.* **1996**, *118*, 6716−6723.

(22) Rong, Y.; Han, H. Monolithic Quasi-Solid-State Dye-Sensitized Solar Cells Based on Graphene-Modified Mesoscopic Carbon−Counter Electrodes. *J. Nanophotonics* **2013**, *7*, 073090.

(23) Wang, H.; Liu, G.; Li, X.; Xiang, P.; Ku, Z.; Rong, Y.; Xu, M.; Liu, L.; Hu, M.; Yang, Y.; et al. Highly Efficient Poly(3-hexlthiophene) Based Monolithic Dye-Sensitized Solar Cells with Carbon Counter Electrode. *Energy Environ. Sci.* **2011**, *4*, 2025−2029.

(24) Xu, M.; Liu, G.; Li, X.; Wang, H.; Rong, Y.; Ku, Z.; Hu, M.; Yang, Y.; Liu, L.; Liu, T.; et al. Efficient Monolithic Solid-State Dye-Sensitized Solar Cell with a Low-Cost Mesoscopic Carbon Based Screen Printable Counter Electrode. *Org. Electron.* **2013**, *14*, 628−634.

(25) Wang, B.; Leung, M. K. H.; Lu, X.-Y.; Chen, S.-Y. Synthesis and Photocatalytic Activity of Boron and Fluorine Codoped TiO_2 Nanosheets with Reactive Facets. *Appl. Energy* **2013**, *112*, 1190−1197.

(26) Wang, Z.; Lv, K.; Wang, G.; Deng, K.; Tang, D. Study on the Shape Control and Photocatalytic Activity of High-Energy Anatase Titania. *Appl. Catal., B* **2010**, *100*, 378−385.

(27) Han, X.; Kuang, Q.; Jin, M.; Xie, Z.; Zheng, L. Synthesis of Titania Nanosheets with a High Percentage of Exposed (001) Facets and Related Photocatalytic Properties. *J. Am. Chem. Soc.* **2009**, *131*, 3152−3153.

(28) Leijtens, T.; Lauber, B.; Eperon, G. E.; Stranks, S. D.; Snaith, H. J. The Importance of Perovskite Pore Filling in Organometal Mixed Halide Sensitized TiO_2-Based Solar Cells. *J. Phys. Chem. Lett.* **2014**, *5*, 1096−1102.

(29) Suarez, B.; Gonzalez-Pedro, V.; Ripolles, T. S.; Sanchez, R. S.; Otero, L.; Mora-Sero, I. Recombination Study of Combined Halides (Cl, Br, I) Perovskite Solar Cells. *J. Phys. Chem. Lett.* **2014**, *5*, 1628−1635.

(30) Dualeh, A.; Moehl, T.; Tétreault, N.; Teuscher, J.; Gao, P.; Nazeeruddin, M. K.; Grätzel, M. Impedance Spectroscopic Analysis of Lead Iodide Perovskite-Sensitized Solid-State Solar Cells. *ACS Nano* **2013**, *8*, 362−373.

(31) Christians, J. A.; Fung, R. C. M.; Kamat, P. V. An Inorganic Hole Conductor for Organo-Lead Halide Perovskite Solar Cells. Improved Hole Conductivity with Copper Iodide. *J. Am. Chem. Soc.* **2014**, *136*, 758−764.

(32) Juarez-Perez, E. J.; Wuβler, M.; Fabregat-Santiago, F.; Lakus-Wollny, K.; Mankel, E.; Mayer, T.; Jaegermann, W.; Mora-Sero, I. Role of the Selective Contacts in the Performance of Lead Halide Perovskite Solar Cells. *J. Phys. Chem. Lett.* **2014**, *5*, 680−685.